An Accurate, Shade Detection-Based Hybrid Maximum Power Point Tracking Approach for PV Systems

Dhanup S. Pillai, *Member, IEEE*, J. Prasanth Ram, A. M. Y. M. Ghias, *Senior Member, IEEE*, Md Apel Mahmud, *Senior Member, IEEE*, and N. Rajasekar, *Senior Member, IEEE*

***Abstract*—Optimizing the operational performance of maximum power point trackers during multiple peak partial shading conditions (PSCs) prevails as a major challenge in photovoltaic power generation. Though many of the newly evolved soft computing and heuristic methods are compatible during PSCs, the need for such techniques in uniform irradiation levels is uncertain because most of these algorithms produce extensive oscillations before converging to the global maximum power point (GMPP). On the other hand, adopting conventional perturb and observe (P&O) algorithm is meritorious to reduce the transient power and voltage oscillations. Therefore, this article presents a proficient hybrid tracking technology that provides an adequate tradeoff between conventional P&O and advanced soft computing techniques by accurately detecting shade occurrences. For which, the uniqueness in the operating point conductance of P&O at the leftmost power peak in the *P–V* curve is utilized. Subsequently, the proposed convention utilizes P&O for two major purposes: to track MPP in uniform irradiance, and to detect PSCs. More importantly, even during PSCs, the detection algorithm is well designed to operate at GMPP with the conventional P&O method itself, and, only for extreme shade cases, flower pollination algorithm is introduced to track GMPP. The pre-eminence of the proposed technology to track GMPP with reduced transient oscillations by discriminating shade occurrences is demonstrated via extensive experimental studies in this article.**

***Index Terms*—Photovoltaic (PV), global maximum power point (GMPP), maximum power point tracking (MPPT), partial shade conditions (PSC), perturb and observe (P&O).**

Manuscript received June 10, 2019; revised September 28, 2019; accepted November 6, 2019. Date of publication November 12, 2019; date of current version February 20, 2020. This work was supported by the Academic Research Fund Tier1 at Nanyang Technological University. Recommended for publication by Associate Editor Y. Xing. *(Corresponding author: N. Rajasekar.)*

D. S. Pillai and A. M. Y. M. Ghias are with the School of Electrical and Electronic Engineering, Nanyang Technological University, Singapore (e-mail: dhanup.pillai@ntu.edu.sg; amer.ghias@ntu.edu.sg).

J. P. Ram is with the Department of Electrical and Electronics Engineering, New Horizon College of Engineering, Bangalore 560103, India (e-mail: jkprasanthram@gmail.com).

M. A. Mahmud is with the Department of Electrical and Electronics, School of Engineering, Faculty of Science Engineering and Built Environment, Deakin University, Geelong, VIC 3220, Australia (e-mail: apel.mahmud@deakin.edu.au).

N. Rajasekar is with the Solar Energy Research Cell, Department of Energy and Power Electronics, School of Electrical Engineering, Vellore Institute of Technology, Vellore 632014, India (e-mail: nrajasekar@vit.ac.in).

Color versions of one or more of the figures in this article are available online at http://ieeexplore.ieee.org.

Digital Object Identifier 10.1109/TPEL.2019.2953242

I. Introduction

THE RAPID reduction in PV panel prices and cutting edge researches on solar photovoltaic (PV) has outreached the common man to visualize solar power at a low cost. Rendered by huge financial supports, PV installations worldwide alone have accounted for annual growth of 103 GW in 2018 [1]. Characterized by its nonlinear current–voltage relationship, the current mismatch between unshaded and shaded PV modules during partial shade conditions (PSCs) contributes to multiple peak occurrences in the output *P–V* characteristics that subsequently hinders smooth *I–V* curve synthesis [2]–[6]. As a result, historical maximum power point tracking (MPPT) methods such as hill climbing [4], [5], perturb and observe (P&O) [7]–[9], and incremental conductance [10], [11] cannot reach global maximum power point (GMPP) during PSCs in most cases. Therefore, to accomplish maximum power generation during PSCs, soft computing techniques such as particle swarm optimization (PSO) [12], improved PSO [13], firefly algorithm [14], random search method [15], artificial bee swarm optimization [16], and flower pollination algorithm (FPA) [17] have been widely attempted.

Though the abovementioned techniques show its prominence and have higher probability to attain GMPP operation in PSCs, these methods are subjected to extensive transient oscillations in its quest to search for GMPP on a broader search space. On the other hand, modern-day PV technologies still deploy the conventional P&O method to track MPP because of the following advantages [3], [5], [18]: relatively simple in operation, computationally efficient, and easy to implement. However, compromising GMPP operation during PSCs leads to huge power loss and reduces the system efficiency [5]. Therefore, the suitable selection of MPPT methods is inevitable. Besides, detecting PSCs also becomes crucial in achieving reliable utilization of soft computing techniques as such techniques are only needed for PSCs. Thus, the development of hybrid tracking techniques that can guarantee an efficient tradeoff between the advantages of conventional and advanced soft computing methods becomes a mandatory obligation for reliable, efficient, and optimal GMPP tracking in PV systems.

Generally, three hybrid tracking approaches are available in the technical literature:

1) Initialize global search using soft computing technique and switch to conventional P&O for local search [19]–[21];

2) Combine two soft computing/conventional techniques to perform both global and local searches [22], [23];
3) Detect partial shade using conventional technique and switch to global search algorithm only during PSCs to locate GMPP [24], [25].

Among the techniques in category 1, a combination of deterministic PSO and conventional P&O is conceptualized in [19], ant colony optimization assisted P&O is developed in [20], and a conventional PSO in combination with adaptive P&O is presented in [21]. The methods in [19] and [20] are advantageous to improve the search mechanism and tracking speed, but both methods cannot always guarantee GMPP operation since switch to P&O has been performed imaginarily without any justification after a predetermined number of iterations, assuming that the particles might have already reached near to GMPP. Whereas integration of the search-skip-judge tool to PSO search space proposed in [21] alleviates this issue to a great extent. Nevertheless, extensive oscillations prior to GMPP convergence limit the practicality of all abovementioned hybrid techniques. Hybrid approaches in category 2 combining two soft computing techniques also have identical limitations. For instance, the hybrid tracking solution developed by integrating the global search ability of differential evolution with conventional PSO in [22] has high switching transients; large power and voltage oscillations; unjustified switching between algorithms; and extensive parameter tuning. In a distinctive approach, the classification capability of artificial neural networks is hybridized with conventional P&O in [23]. However, the power difference constraint considered to locate GMPP is erroneous as the power difference during multiple peak cases is highly related to the shade profile. Thus, the methods listed in categories 1 and 2 are neither reliable nor efficient for optimal tracking, and also, are not proficient to discriminate between uniform irradiance and PSCs.

Methods in category 3 [24], [25] detect PSCs and employ soft computing algorithms conditionally, which eventually eliminate unnecessary oscillations. Among these, identical techniques are accessible in [24], where conventional P&O is hybridized with PSO and Fireworks algorithms (FWA), respectively. However, the voltage limits used for shade detection in [24] is likely to fail when the number of unshaded modules in a PV string is higher than the shaded modules, whereas the method proposed in [24] involves complex computations and is not compatible during PSCs that occur in low irradiance conditions. More importantly, both the techniques are hypothesized for string inverters (distributed MPPT) and are not suitable for central inverter topologies (single MPPT). Unlike above, [25] performs shade detection by theoretically estimating the change in irradiation levels with respect to an intermediate point "$0.5\,V_{\rm oc}$" in the *P–V* curve. However, the assumptions used for setting the thresholds limits are not validated, and moreover, the voltage limit assumption of "$\leq 0.8\,V_{\rm oc}$" used to locate GMPP fails during numerous shade conditions. Above all, the criterion used to identify P&O settling is not specified in either of the above methods. From the extensive literature study conducted, three primary challenges that require immediate attention are evident for hybrid tracking technologies: accurate detection of shade occurrence; handling transient oscillations; and compatibility with string as well as central inverter topologies.

In the above context, though not hybrid, global heuristic techniques that attempt to achieve GMPP operation are also studied [26]–[29]. For instance, similar adaptive P&O techniques based on an improved voltage band selection and voltage window search are devised in [26] and [27], respectively. Even though both techniques are highly realistic, the former does not always attain maximum power if the GMPP is the leftmost power peak (LPP) in the *I–V* curve, whereas the latter fails to discriminate between GMPP and local maximum power point if the power difference is minimal. Distinctively, individual module voltages are measured in [28] to identify GMPP during PSCs. However, module-level sensor requirement and its incompatibility toward PSCs characterized by more than three power peaks limit its application to large scale PV installations. The *I–V* curve approximation technique proposed in [29] cannot guarantee GMPP operation if the global power point is located to an operating point with voltage less than single module MPP voltage. The method is also: computationally complex; requires extensive sampling of the *I–V* curve, particularly during PSCs with a higher number of power peaks; and needs an accurate measurement of the open-circuit voltage of the array during each reinitialization step. Therefore, high-precision, fast-speed digital processors are mandatory for its practical implementation that eventually increases the overall cost of the PV system. In addition, intermittent samplings needed at various points in the *I–V* curve and the inability to differentiate between PSCs and uniform irradiance are also major concerns.

Addressing all observed drawbacks, a new, novel, and accurate shade detection based hybrid tracking methodology compatible for all inverter topologies is designed and implemented in this work. The proposed concept for shade detection primarily evolves from the uniqueness of the LPP in the *I–V* curve and is predominantly based on the operating point conductance of P&O at LPP. Furthermore, by monitoring the voltage levels at LPP along with the conductance value, the technology is well efficient to discriminate between uniform irradiance, temperature variations, and PSCs. Subsequently, either P&O or FPA is devised to track GMPP. More importantly, the proposed methodology is proficient to locate GMPP during PSCs characterized by two power peaks. Therefore, even in shade conditions, the method shows its potential to track GMPP with P&O itself. Thus, the decision to switch to global tracking mode is competently made to avoid needless switching between two algorithms and thereby, FPA is used to track GMPP during extreme shade conditions only. Note that, even though this work uses FPA, any such competent global search techniques can also be utilized as alternatives. Extensive experiments pertinent to different PV array configurations are performed and presented in this article to demonstrate the superiority of the proposed method.

II. Behavioral Study on PV Array Characteristics to Develop Shade Detection Rules

The previous discussions portray the importance of developing an efficient MPP tracking scheme that identifies shade and discriminates uniform irradiance conditions. In order to develop accurate shade detection rules, it is imperative to understand the unique PV array characteristics during various practical operating conditions. Therefore, to realize some critical observations on the PV array characteristics during normal and PSCs, a PV

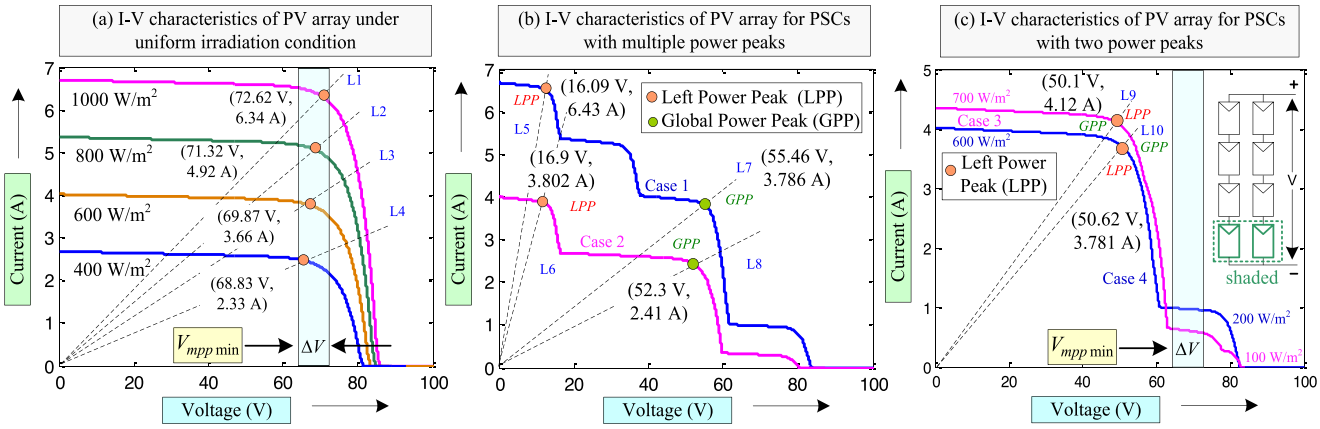

Fig. 1. *I–V* characteristics of the PV array: (a) uniform irradiation conditions and (b) partially shaded conditions with multiple power peaks; and (c) partial shade conditions with two power peaks.

array of "4×2" size is built and simulated using the conventional single diode PV model [30] in a MATLAB platform. For analysis, Shell SM55 PV module having the following data sheet specifications is considered: power at MPP $(P_{\rm mp}) - 55$ W, voltage at MPP $(V_{\rm mp}) - 18.1$ V, current at MPP $(I_{\rm mp}) - 3.17$ A, open-circuit voltage $(V_{\rm oc}) - 21.4$ V, and short-circuit current $(I_{\rm sc}) - 3.58$ A. The simulated *I–V* curves obtained for uniform irradiance, PSCs with multiple (more than two) peaks and PSCs with two power peaks shown in Fig. 1(a)–(c) are separately analyzed.

A. *Observing the Uniqueness of LPP in the* I–V *Characteristics*

In order to distinguish uniform irradiance from PSCs, a fundamental examination on array *I–V* characteristics is inevitable. For which, the constructed "4×2" PV array is first exposed to a variety of uniform irradiances from 1000 to 400 W/m^2, and the respective *I–V* curves characterized by single power peaks as well as corresponding load lines L1–L4 are depicted in Fig. 1(a). It can be seen that, at MPP, the array operates at 72.62 V and 6.34 A at 1000 W/m^2, whereas it reduces to 68.83 V and 2.33 A at 400 W/m^2. This particular observation deduces that the power drop during uniform irradiance is predominantly due to the reduction in current only, whereas the drop in voltage magnitude is marginal, i.e., nearly equal to 5% (3.8 V in the present case) of its nominal value at standard test conditions (STC). Furthermore, to incorporate the effect of irradiance below 400 W/m^2, an additional drop of 5% can be considered as explained in [18]. Therefore, the drop in voltage magnitude of any PV array operating in uniform irradiance conditions is expected not to be lesser than 10% of its nominal MPP voltage. In mathematical terms, if $V_{\rm mpp\ nom}$ is the nominal voltage of a PV array at STC conditions, the minimum voltage at which it can operate during uniform irradiance conditions, $V_{\rm mpp\ min}$ is given by

$$V_{\rm mpp\,min} = V_{\rm mpp\ nom} - 0.1V_{\rm mpp\ nom} = 0.9V_{\rm mpp\ nom}. \quad (1)$$

With the essential understanding of uniform irradiance operation, the effect of PSCs on the array *I–V* characteristics is also evaluated. Due to the presence of bypass diodes, multiple peaks are introduced to *I–V* characteristics when there is nonhomogenous irradiation falling on different PV modules. Two such partial shading cases having multiple power peaks illustrated in Fig. 1(b) are considered for a detailed analysis. Four power peaks are created in case 1 by applying four different irradiation levels corresponding to each row in the considered "4×2" PV array: 1000, 800, 600, and 200 W/m^2, whereas case 2 attributes three different irradiation levels 600 W/m^2 (one row), 400 W/m^2 (two rows), and 200 W/m^2 (one row). For both cases, the load lines corresponding to the LPP (L5, L6) and GMPP (L7, L8) are drawn to indicate the respective IV co-ordinates.

The uniqueness of LPP occurrence in *I–V* characteristics during PSCs is now elaborated. Typically, LPP represents the maximum current that can be delivered by the PV array after bypassing all shaded modules. Once the shaded PV modules get bypassed, the voltage at LPP is constituted by the unshaded modules only. This can be well observed in the above shade cases where the operating voltage and current at LPP for cases 1 and 2 are 16.09 V and 6.43 A, and 16.9 V and 3.802 A, respectively. For clarity, partial shade case 1 is further investigated. Since for case 1, only one row in the "4×2" PV array receives maximum irradiation of 1000 W/m^2 (STC), the voltage and current at LPP marked in Fig. 1(b) is approximately equal to the voltage of one unshaded module (in a string) and the algebraic sum of unshaded module currents in two parallel two strings. Thus, the LPP for case 1 is located to a point in the *I–V* curve that corresponds to the net STC current and one PV module MPP voltage approximately. Identical results can also be seen for case 2 where LPP current is the array current at maximum irradiance, 600 W/m^2. To generalize the above observations, the following mathematical equations are derived for PSCs.

If $V_{\rm mp\ us}$ is the MPP voltage of an unshaded PV module receiving maximum irradiance and $N_{\rm us}$ is the number of unshaded modules in a PV string, then the voltage at LPP, $V_{\rm Lpp}$ is given by

$$V_{\rm Lpp} = N_{\rm us} \times V_{\rm mp\ us}. \quad (2)$$

Similarly, If $I_{\rm mp\ us}$ is the MPP current of an unshaded PV module receiving maximum irradiance in a PV string and $N_{\rm us\,string}$ is the number unshaded parallel strings, then current

at LPP, I_{Lpp} is given by

$$I_{\mathrm{Lpp}} = N_{\mathrm{us\ string}} \times I_{\mathrm{mp\ us}}. \tag{3}$$

B. Significance of Conductance Value at LPP for Shade Detection and Classification

From the extensive analysis carried out, it is imperative that the array output characteristics during PSCs and uniform irradiance conditions are unique. Two critical inferences observed during PSCs are as follows.

1) During the operational transition of a PV array from STC to uniform irradiance conditions, the percentage change in LPP voltage is less significant compared to the change in current.
2) The magnitude of LPP voltage during PSCs in an *I–V* curve is very low compared with uniform irradiance conditions.

As a result, the percentage reduction in power at LPP during PSCs is primarily due to the drastic reduction in operating voltage, whereas the same for uniform irradiance is due to the large reduction in current levels. Here, it is essential to note that LPP mentioned for uniform irradiance refers to its respective unique MPP itself. In summary, if $V_{\mathrm{Lpp\ unf}}$ and $V_{\mathrm{Lpp\ psc}}$ indicate the LPP voltages at uniform irradiance and PSCs, respectively, the following mathematical relation is valid for all PV arrays

$$V_{\mathrm{Lpp\ psc}} \ll V_{\mathrm{Lpp\ unf}}; \text{for PSCs.} \tag{4}$$

Now, the voltage range of V_{Lpp} during uniform irradiance and PSCs can be easily derived from (1) and (4) as

$$V_{\mathrm{mpp\ nom}} \geq V_{\mathrm{Lpp}} \geq 0.9\ V_{\mathrm{mpp\ nom}};\ \text{for uniform irradiance} \tag{5}$$

$$V_{\mathrm{Lpp}} \ll 0.9 V_{\mathrm{mpp\ nom}}; \text{for PSCs.} \tag{6}$$

In order to incorporate the effect of current at LPP along with the voltage, the conductance value at LPP expressed as the ratio of LPP current to LPP voltage is now introduced and the nominal conductance of a PV array, G_{nom} that corresponds to STC is defined by the following equation

$$(I_{\mathrm{mpp\ module}} \times n)/(V_{\mathrm{mpp\ module}} \times m) = G_{\mathrm{nom}} \tag{7}$$

where n represents the number of parallel strings, m is the number of series-connected PV modules in a string, and $I_{\mathrm{mpp\ module}}$ and $V_{\mathrm{mpp\ module}}$ are the MPP current and voltage of a PV module, respectively.

Also, the conductance value at LPP in an *I–V* curve, G_{Lpp} can be calculated as

$$G_{\mathrm{Lpp}} = \frac{I_{\mathrm{Lpp}}}{V_{\mathrm{Lpp}}}. \tag{8}$$

To exemplify the effect of LPP conductance, its peculiar nature at uniform irradiance and PSCs is carefully studied for various operating conditions illustrated in Fig. 1(a) and (b). At STC in Fig. 1(a), the nominal conductance value calculated as per (7) for the considered "4×2" PV array is 0.087. Undoubtedly, for uniform irradiation levels less than 1000 W/m^2, the change in voltage is negligible compared to highly diminishing current levels, and hence, the LPP conductance in those conditions will be lesser than that at STC. For instance, the LPP conductance value calculated using (8) for 800, 600, and 400 W/m^2 are 0.068, 0.052 and 0.034, respectively. On the other hand, under PSCs, the voltage at LPP will be very less compared to uniform irradiance, whereas the operating current at LPP will be the maximum deliverable array current. Hence, for case 1 and case 2 in Fig. 1(b), the LPP conductance is significantly high compared to its nominal value of 0.087, and is 0.38 and 0.22 for case 1 and case 2, respectively. The observation can be generalized as follows:

$$G_{\mathrm{Lpp}} \leq G_{\mathrm{nom}}; \text{for uniform irradiance} \tag{9}$$

$$G_{\mathrm{Lpp}} \gg G_{\mathrm{nom}}; \text{for PSCs with multiple power peaks.} \tag{10}$$

The conclusions derived in (5), (6), (9), and (10) indicate that PSCs with multiple power peaks can be easily detected and discriminated from uniform irradiance conditions by monitoring the magnitude of LPP voltage and conductance values.

C. Significance Detecting Shade and Identifying GMPP in PSCs With Two Power Peaks

As multiple peak shade occurrences can be accurately detected using the above procedure, there are peculiar shades that are still hard to detect, especially those with two power peaks. Hence, two peculiar PSCs, cases 3 and 4 having two power peaks shown in Fig. 1(c) are explicitly considered to analyze such undetectable scenarios. As clearly indicated in Fig. 1(c), both of the cases evaluated are unique compared with the earlier PSCs in the following ways: first, to allow maximum possible LPP voltage, only one row is assumed to be shaded (100 W/m^2 for case 3 and 200 W/m^2 for case 4); and second, to reduce the LPP current, the maximum irradiance falling on all unshaded modules are assumed to be lesser than that at STC (700 W/m^2 for case 3 and 600 W/m^2 for case 4). While the objective is to reduce the LPP conductance during PSCs, cases 3 and 4 now occur with LPP conductance values 0.081 and 0.074, respectively, which is lesser than its nominal value (G_{nom}) of 0.087. Furthermore, it can be observed that the particular finding violates the conductance limits defined earlier in (10) for multiple peak PSCs. It must be noted here that, though the conductance limit is violated, the LPP voltages 50.1 and 50.62 V obtained for both PSCs are well below $V_{\mathrm{mpp\ min}}$ (65 V), which is precisely in line with the voltage limits derived in (5) and (6) to differentiate between uniform irradiance and PSCs.

In addition to the previous annotations, some interesting fundamental aspects are also evident from the peculiar practical shade cases considered in Fig. 1(c). It can be visualized that both the LPPs indicated in cases 3 and 4 are GMPPs itself. This is so because the majority of the modules are not shaded constituting to a higher voltage at LPP co-ordinates, which eventually reduces the conductance value. As the unshaded modules define the LPP co-ordinates in an *I–V* curve, this will only happen if the LPP itself is the GMPP in a two-peak *P–V* curve. Undoubtedly, the LPPs shown in cases 3 and 4 would have been local peaks if the majority of the PV modules were shaded. Therefore, once the LPP becomes a local peak in a two-peak curve, the LPP conductance will increase due to low LPP voltage magnitudes (less number of unshaded modules). In those cases, PSCs can be easily detected using the previously derived threshold limits expressed in (6) and (10). Principally, two critical evaluations can summarize the fundamental study

TABLE I
GENERALIZED LPP CONSTRAINTS AT VARIOUS OPERATING CONDITIONS OF A PV ARRAY

Sl. No.	V_{Lpp} (V)	G_{Lpp}	No. of Power peaks	Type of LPP peak	Operating Condition
1	$V_{mpp\ nom}$	G_{nom}	One	Global	Ideal
2	$< V_{mpp\ nom}$ & $\geq V_{mpp\ \min}$	$\leq G_{nom}$	One	Global	Normal (uniform irradiance)
3	$< V_{mpp\ nom}$ & $< V_{mpp\ \min}$	$\leq G_{nom}$	Two	Global	Partially Shaded
4	$< V_{mpp\ nom}$ & $< V_{mpp\ \min}$	$> G_{nom}$	Multiple	Local/Global	Partially Shaded

performed: first, PSCs having two power peaks with lesser LPP conductance value than $G_{\rm nom}$ will always occur at an LPP voltage less than $V_{\rm mpp\ min}$; and second, LPPs with conductance value less than $G_{\rm nom}$ and voltage value less than $V_{\rm mpp\ min}$ are always GMPPs in *I–V* curves characterized by two power peaks. In general, the following mathematical relation can be derived to identify PSCs with two power peaks having the same LPP and GMPP

$$G_{\rm Lpp} \leq G_{\rm nom} \text{ and } V_{\rm Lpp} \ll 0.9\ V_{\rm mppnom}; \quad \text{for PSCs with two power peaks having LPP as GMPP.} \tag{11}$$

It is worth mentioning that no techniques available till date in the literature can identify GMPP during PSCs. The proposed strategy can accurately locate GMPP in most practical two-peak PSCs. In addition, the method is also proficient to detect all PSCs irrespective of the number of peaks based on the conclusions derived.

D. Consolidated Shade Detection Rules

The extensive behavioral study performed in the previous sections to analyze the signatures of various operating conditions of a PV array suggests that PSCs can be accurately detected by monitoring the LPP conductance and voltage values in an *I–V* or *P–V* curve. Also, the location of GMPP can also be identified in specific cases by utilizing the fundamental concepts derived. All findings and observations discussed so far are consolidated to derive the shade detection rules presented in Table I. Furthermore, to validate the findings, numerous shade cases have been simulated with the considered 4×2 PV array and the respective conductance and voltage values are plotted in Fig. 2. The figure illustrates that all PSCs occurring in a PV array can be detected by monitoring the magnitude of only two parameters at LPP: voltage, and conductance.

III. PROPOSED HYBRID TRACKING TECHNIQUE

A new hybrid tracking scheme combining conventional P&O and recently evolved FPA [17] is conceptualized in this work. In order to implement efficient tracking with less switching transients, two essential features are introduced to impart intelligence to the tracking flow. First, the operating condition of the PV array is identified using the LPP constraints expressed in Table I, and then, a suitable algorithm is selected to track the GMPP. It is important to note that selection is convincingly made to avoid unnecessary switching between tracking algorithms. The sequential steps employed for tracking are explained in detail to understand the effectiveness of the proposed technique.

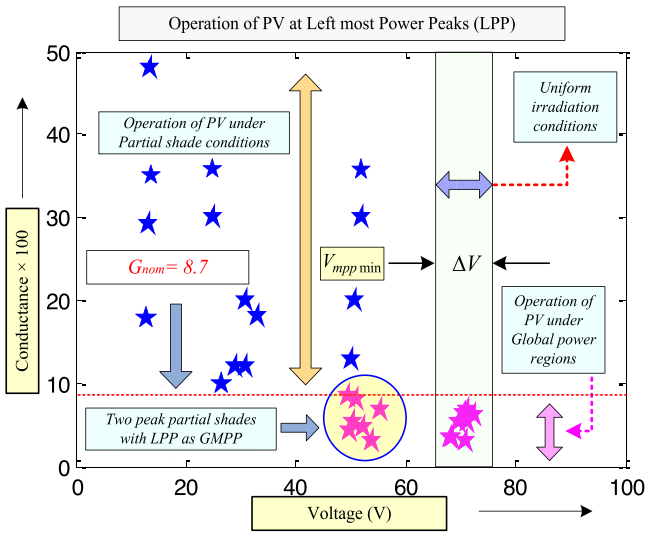

Fig. 2. LPP conductance and voltage values obtained for various test cases for the considered PV array.

A. Initiating Conventional P&O to Track LPP Co-Ordinates

The proposed hybrid tracking technique efficiently utilizes the operating behavior of the conventional P&O algorithm [18] to identify the operating conditions of any PV array. In order to track LPP and monitor the constraints derived in Table I, the proposed tracking scheme starts by initializing the conventional P&O MPPT method from the left-hand side of an *I–V* curve. Thus, to guarantee the LPP operation, an initial duty cycle (D) of 0.85 is selected to track the nearest MPP. It is important to note that, as P&O tracks MPP by fixed voltage perturbations, it settles to LPP without transient oscillations. At the same time, LPP parameters defined in Table I are used to identify the particular operating condition.

1) Formulation of Mathematical Constraints to Identify Settling of P&O to LPP: The inherent three-point behavior of the P&O method imposes considerable challenges in identifying the settled LPP operating parameters. Since there are three different LPP co-ordinate values possible, the detection rules illustrated in Table I may be violated under such circumstances. Hence, it becomes mandatory to identify when P&O settles and at what LPP co-ordinates does it operate. This particular behavior is expressed with the help of a three-point P&O waveform depicted in Fig. 3, where the typical three-point appearance is presented. After performing various experimentations, it is observed that P&O settling can be identified from its typical triple point behavior by monitoring its voltage changes. Based on the voltage levels presented in Fig. 3, two rules are formulated

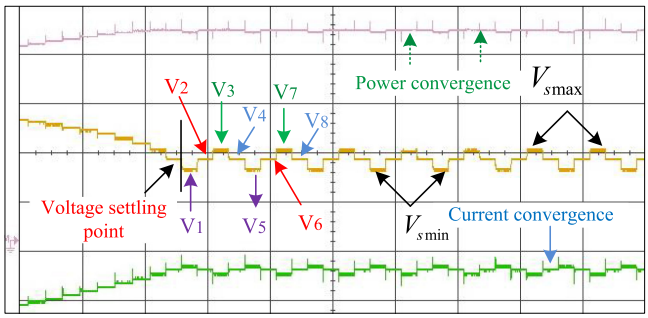

Fig. 3. Experimental waveform to analyze the behavior of P&O settling.

to accurately identify the settled operation and the respective steady-state operating voltage of P&O. According to Fig. 3, if $v_1, v_2 \ldots, v_n$ are the instantaneous voltages, P&O is settled if the following voltage condition is satisfied:

$$v_i - v_{(i-4)} = v_{(i+1)} - v_{((i+1)-4)} = v_{(i+2)} - v_{((i+2)-4)}; \quad \text{for } i \geq 5. \tag{12}$$

Once P&O settling is confirmed, the settled LPP operating voltage can be calculated by

$$V = (V_{s\,\max} + V_{s\,\min})/2. \tag{13}$$

In rare cases, P&O also generates a five-point steady-state operating behavior if the signal-to-noise ratio is low. In such conditions, (12) might fail to identify P&O settling. Therefore, (12) is improved by comparing every sixth instant of the P&O voltage as

$$v_i - v_{(i-6)} = v_{(i+1)} - v_{((i+1)-6)} = v_{(i+2)} - v_{((i+2)-6)}; \quad \text{for } i \geq 7. \tag{14}$$

It is important to mention that either (12) or (14) must be satisfied for the reliable identification of P&O settling. Note that for brevity, the five-point behavior is not shown and can be easily understood from Fig. 3 itself.

2) Reinitialization of P&O to Sense Irradiance Change and Counteract Temperature Effect: Once the initialization is made with P&O, the algorithm must be capable of deciding when to retrigger P&O to detect a possible shade occurrence. To allow this to happen, it is necessary to sense the change in irradiation levels falling on the PV array. Therefore, P&O is retriggered to check for a possible shade occurrence according to the voltage and current thresholds defined using the following equations

$$\frac{V_{\rm PV}(k) - V_{\rm PV}(k-1)}{V_{\rm PV}(k)} \geq 0.2 \tag{15}$$

$$\frac{I_{\rm PV}(k) - I_{\rm PV}(k-1)}{I_{\rm PV}(k)} \geq 0.1 \tag{16}$$

where $V_{\rm PV}(k)$ and $I_{\rm PV}(k)$ are the P&O voltage and current at kth iteration whereas $V_{\rm PV}(k-1)$ and $I_{\rm PV}(k-1)$ are the P&O voltage and current at $(k-1)$th iteration. For detailed discussions on the threshold limits above, readers can refer to [14]–[17]. Another question that may arise now is the effect of temperature on LPP parameters defined in Table I. Since the proposed indicators for shade detection at LPP is also dependent on the operating temperature of PV modules, it is necessary to distinguish between irradiance changes and temperature variations of the PV array. In this context, criterions defined in (14) and (15) guarantee that the reinitialization process will only be triggered during irradiance changes. While, during temperature variations, the change in voltage and current corresponding to the present and previous iterations might not be substantial enough to initiate the reinitialization sequence. This is justified because temperature variations are not instantaneous with the change in irradiation levels and the transition is as low as 0.2 °C–0.3 °C per step change in irradiation [18].

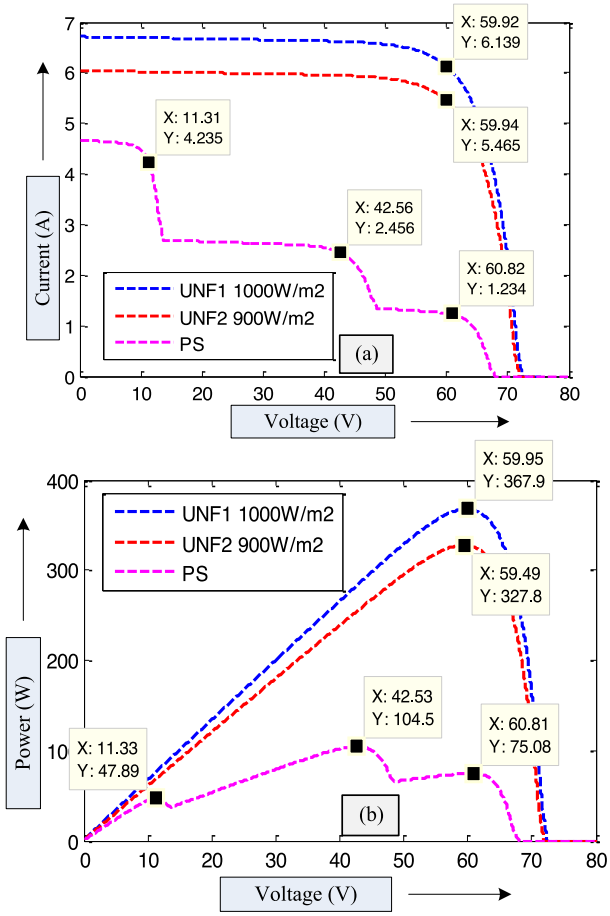

Fig. 4. Analysis on the effect of irradiance change on a 4×2 PV array operating at 75 °C. (a) *I–V* and (b) *P–V* characteristics.

B. Resolving False PSC Detection at High Operating Temperatures

The reinitialization constraints derived above ensure that P&O does not respond to small temperature variations of the PV array. However, an irradiance change would retrigger the thresholds defined in (15) and (16) if the PV array is already at an operating point with high temperatures. This could possibly increase the conductance value above $G_{\rm nom}$ as temperature changes are associated with a large drop in voltage with barely no change in current levels. To illustrate this scenario, a 4×2 PV array (same as for earlier cases) operating at 1000 W/m^2 and 75 °C, as shown in Fig. 4, is considered. Assuming that P&O has not been reinitialized, an irradiance change to 900 W/m^2 at this point will reinitialize the algorithm to settle to (56.6 V, 5 A)

TABLE II
PROPOSED HYBRID TRACKING TECHNIQUE

Sl. No.	P&O voltage (V)	P&O conductance (G)	Voltage change $\lvert\Delta V\rvert$	Identified MPP	Decision
1	$V_{mpp\ nom}$	G_{nom}	-	Global	Continue P&O
2	$< V_{mpp\ nom}\ \&\ \geq V_{mpp\ \min}$	$\leq G_{nom}$	-	Global	Continue P&O
3	$< V_{mpp\ nom}\ \&\ < V_{mpp\ \min}$	$\leq G_{nom}$	-	Global	Continue P&O
4	$< V_{mpp\ nom}\ \&\ < V_{mpp\ \min}$	$> G_{nom}$	$< 0.7 V_{mpp\,module}$	Global	Continue P&O
5	$< V_{mpp\ nom}\ \&\ < V_{mpp\ \min}$	$> G_{nom}$	$> 0.7 V_{mpp\,module}$	Local/Global	Switch to GMPP method

with a conductance value of 0.092 above $G_{\rm nom}$, which leads to false detection of a PSC. However, recalling the observation derived in (4), the instantaneous change in LPP voltage due to PSCs will be substantially high compared to uniform irradiance conditions. Undoubtedly, irrespective of the shade profile, all PSCs are bound to cause an instantaneous reduction of at least one module voltage $V_{\rm mpp\ module}$ at LPP. This is guaranteed because LPP voltage is the net PV array voltage available after bypassing all shaded modules (see PS1 in Fig. 4 generated for a random shade pattern by providing 700 W/m^2 for two modules, 500 and 200 W/m^2 for one module each in a string). Thus, pertinent to the voltage change (Δv) observed by P&O, normal irradiance changes and PSCs can be reliably differentiated even if the conductance value is above $G_{\rm nom}$. Taking into account the overall voltage drop possible due to temperature as well as irradiance changes, a limit of $0.7\ V_{\rm mpp\ module}$ is set to derive the following thresholds to identify PV array operating conditions at high temperatures

$$|\Delta V| \geq 0.7\ V_{\rm mppmodule}\ \&\ G > G_{\rm nom};\ \text{for PSCs} \tag{17}$$

$$|\Delta V| < 0.7\ V_{\rm mppmodule}\ \&\ G > G_{\rm nom};\ \text{for uniform irradiance} \tag{18}$$

C. Developing the Hybrid Tracking Scheme Based on Settled P&O Operating Points

Any reliable hybrid tracking technology proposed for GMPP tracking must accurately decide when to shift from P&O and switch to a GMPP method. In this context, the operating condition of any PV array can easily be identified with respect to P&O voltage and conductance at its settled operating points since P&O accurately operates at LPP in an *I–V* curve. Based on the P&O parameters operating at LPP, a suitable MPPT algorithm is initiated to guarantee GMPP operation. In principle, from Table I, it is evident that P&O is no longer reliable for tracking GMPP if the operating conductance is above $G_{\rm nom}$ and for such cases, a global search technique must be invoked. For other cases, P&O can track GMPP by itself. Thus, pertinent to the uniqueness of LPP co-ordinates in an *I–V* curve, a new hybrid tracking scheme is designed and presented in Table II. Note that the effect of temperature derived in (17) and (18) is also incorporated in Table II. Also, from Tables I and II, it is interesting to note that the proposed method possesses a hidden intelligence to differentiate global peaks during certain PSCs with two power peaks. This intelligence convincingly reduces the computational burden and switching transients involved with all hybrid methods proposed in the literature.

D. Application of FPA for GMPP Tracking

As indicated in Table II, if the settled V, G, and $|\Delta V|$ of P&O are $< V_{\rm mpp\ min}$, $> G_{\rm nom}$, and $> 0.7\ V_{\rm mpp\ module}$, respectively, a global search algorithm is needed to track GMPP. The recently evolved swarm-based FPA [17] is deployed for this purpose in the proposed work. Compared with other techniques in the literature, FPA is meritorious in the following aspects [17]: reduced transient oscillations, excellent tradeoff between local and global search processes, dedicated design incorporating both search processes in one iteration itself, guaranteed randomness among solutions, and flexible parameter tuning. For brevity, only a brief overview of the two design rules followed to implement FPA is provided in this article, whereas for an in-depth understanding of the control rules and parameter tuning, readers are suggested to refer [17].

Rule 1: Biotic or cross-pollination represents the global search process where a levy flight is accompanied to transfer the pollen. The generalized mathematical equation to represent cross-pollination is given as

$$x_i^{k+1} = x_i^k + L(g\text{best} - x_i^k) \tag{19}$$

where i denotes iteration number, k represents the pollen number, $g$best refers to the current best solution obtained in a set of pollens, and L is the associated levy factor that helps in the transfer of pollens. Since the transfer of pollens follow Levy distribution, the flight in pollen is represented by Levy distribution function and given as follows:

$$L = \frac{\lambda\Gamma(\lambda)\sin(\pi\lambda/2)}{\pi}\frac{1}{S^{1+\lambda}}(S \gg S^0 > 0) \tag{20}$$

where $\Gamma(\lambda)$ is the standard gamma distribution function applicable for large step size greater than zero $(S \gg S^0 > 0)$. Based on the trial and error method, the value λ is set to 1.5 to ensure faster convergence.

Rule 2: Abiotic or self-pollination replicates the local search (pollination) process. The mathematical realization for local pollination is given as

$$x_i^{k+1} = x_i^k + \varepsilon(x_m^k - x_j^k) \tag{21}$$

where x_m^k and x_j^k correspond to different pollens of the same species and ε (epsilon) characterize the local search in distribution $\varepsilon \in [0, 1]$.

Note that the switching between the pollination processes is controlled by probability switch $P \in [0, 1]$, and in most cases, P is kept to an optimal value of 0.8. To summarize, the various steps involved in the proposed hybrid tracking algorithm is

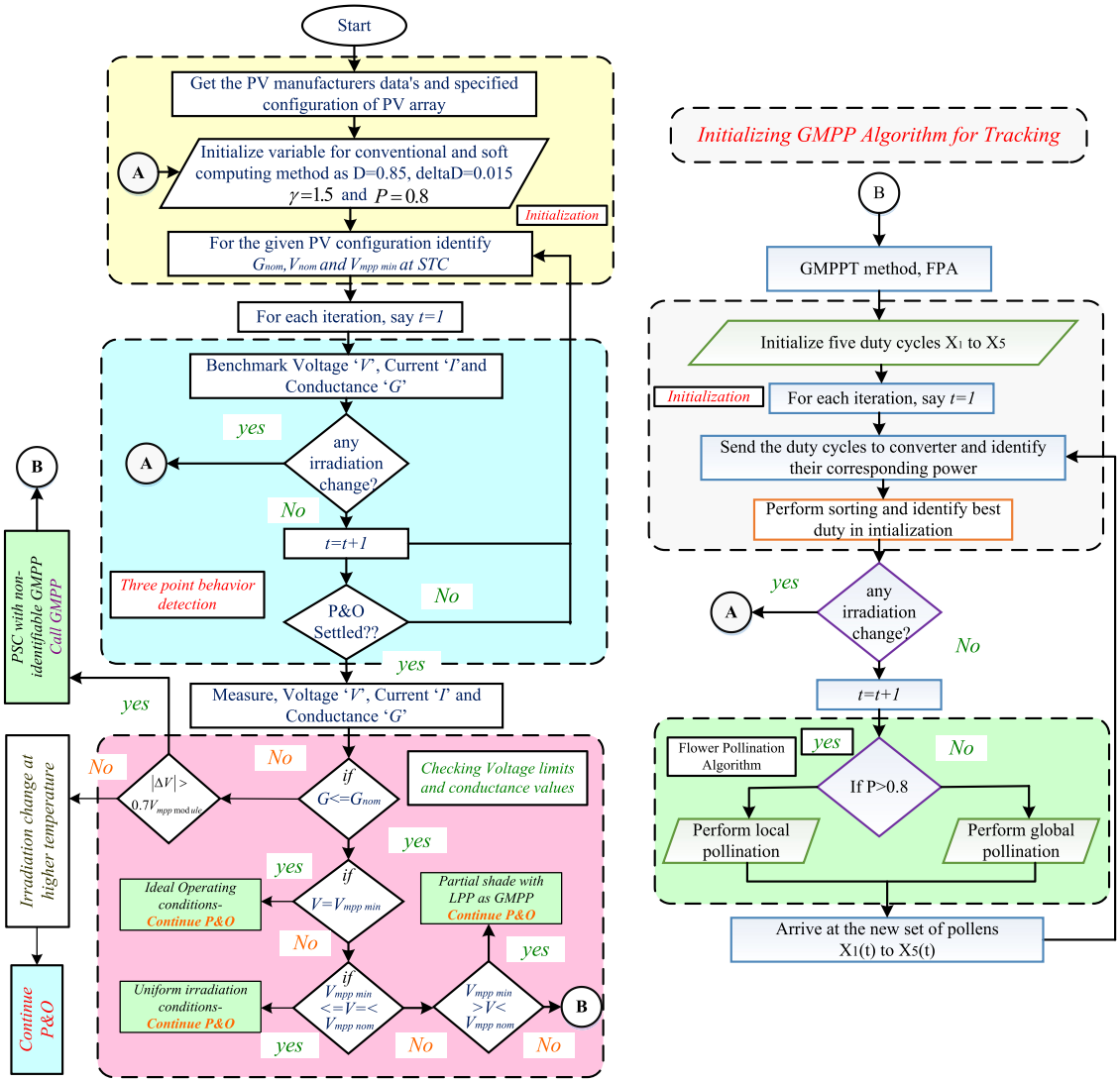

Fig. 5. Flowchart representing the proposed hybrid tracking algorithm.

consolidated and is expressed in the form of a flow chart in Fig. 5.

IV. Experimental Results and Discussions

To validate the proposed hybrid tracking algorithm in real time, a laboratory prototype is built and tested. The schematic and experimental setup showing the proposed hybrid MPPT control is depicted in Fig. 6(a) and (b), respectively. For experimentation, a single-stage dc–dc power conversion unit is designed using a boost converter to implement the proposed MPPT algorithm. The converter design specifications are illustrated in Table III. Note that, though interleaved converters [31] are more advantageous, the proposed system considers a simple boost topology as implementing MPPT to interleaved converters is extremely difficult. Now, to emulate the PV array *I–V* characteristics in real time, a multipurpose CHROMA 62050H PV simulator is employed. The hybrid tracking scheme incorporating the threshold limits defined in Table II is coded using an ARDUINO UNO controller for execution. With two timer circuits, ARDUINO can switch up to a frequency of 10 kHz, and, the sampling interval selected for each duty cycle is 400 ms. Also, LEM high-precision sensors LA55P and LV25P are installed for accurate current and voltage sensing whereas, for isolation purpose, TLP250 driver circuit board is utilized.

TABLE III
Converter Design Specifications

Sl. No	Parameter	Value
1	Switching Frequency	10KHz
2	Inductor	0.5mH
3	Capacitor	450V,100uF
4	Load Resistance	10A,100 ohm

In order to verify the compatibility of the proposed hybrid MPPT algorithm, experimentations are performed for two PV arrays having different configurations: "3 × 2" and "4 × 2" PV array. Different uniform and PSCs are simulated to identify the operating characteristics of each PV array and the respective *I–V* patterns are programmed into the PV simulator in real time for testing the proposed algorithm. Furthermore, validation is done

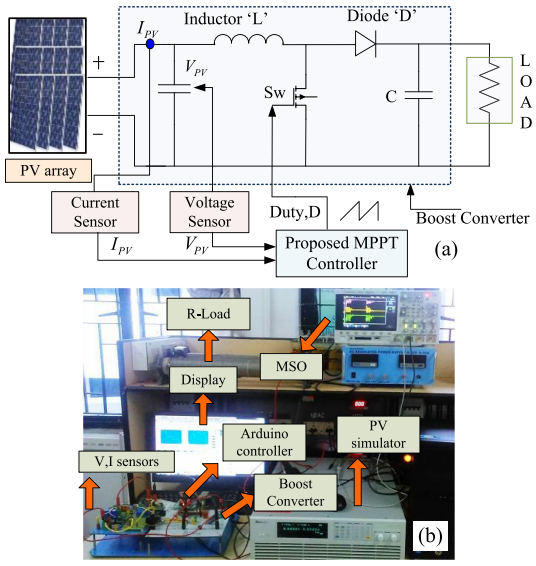

Fig. 6. Experimental Setup: (a) Schematic and (b) designed laboratory prototype.

TABLE IV
IRRADIATION PROFILE FOR A 3 × 2 PV ARRAY

Pattern	Irradiation value in W/m^2		
	Row 1	Row 2	Row 3
UNF1	1000	1000	1000
PS1	1000	1000	700
UNF2	600	600	600
PS2	600	600	300
PS3	700	300	200

for various cases considering the operational transition of the PV array from one condition to another. Moreover, to substantiate the effectiveness of the technique proposed, each hardware result obtained is compared with the widely deployed PSO technique. For all experiments performed, P&O MPPT is initialized with a duty cycle of 0.85 to track LPP and is reinitialized by the threshold limits defined in (15) and (16) to sense the irradiance changes.

A. GMPP Tracking Experiments on a 3 × 2 PV Array

To demonstrate the performance of the proposed hybrid MPPT concept, a 3 × 2 PV array is constructed using SM55 PV modules having the data sheet specifications conveyed in Section II. For extensive analysis, five different operating conditions are simulated with various irradiation profiles and the corresponding *I–V* and *P–V* curves are shown in Fig. 7(a) and (b), respectively. To clearly visualize the voltage, current, and power variations, all the power peaks are properly indicated with their respective electrical coordinates. The irradiation patterns considered to attain the respective characteristics are illustrated in Table IV for a better understanding. At STC (Case 1—UNF1), the array operates with *I–V* coordinate values 6.34 A and 54.38 V. Therefore, for the considered configuration, the value of $V_{\text{mpp nom}}$, $V_{\text{mpp min}}$, and G_{nom} are 54.38 V, 48.9 V, and 0.12, respectively. Now, the performance of the proposed hybrid MPPT is evaluated by considering the following possible

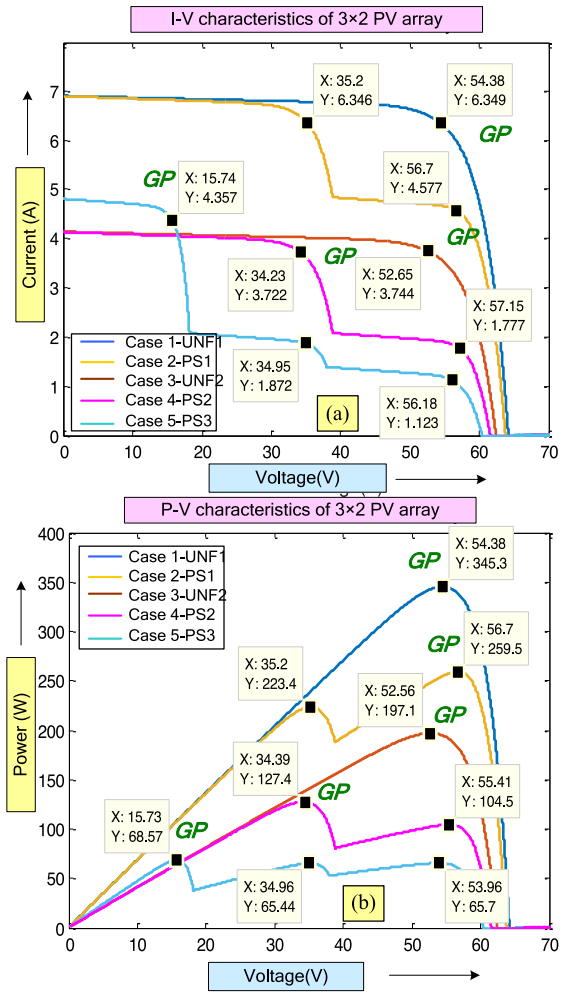

Fig. 7. Different operating conditions considered for 3 × 2 PV array: (a) *I–V* and (b) *P–V* characteristics.

operational transition cases of the PV array: UNF1–UNF2; UNF1–PS1; PS1–PS2; UNF2–PS3; and PS1–PS2–PS3.

1) Experimental Investigation—Case 1. Operational Transition From UNF1 to UNF2: The hardware realization for this sequence using the proposed hybrid MPPT and PSO algorithms are shown in Fig. 8(a) and (b), respectively, where each pattern is run for 50 s and as can be visualized from the results, both methods easily track the single GMPP peak. For UNF1, when initialized with 0.85 duty cycle, P&O settles to the leftmost MPP (single in this case) located at 54.3 V having a conductance value of 0.12. Upon settling, based on the limits specified in Table II, P&O identifies the global peak and hence, continues at the same operating point. Meanwhile, when the irradiation reduces to 600 W/m^2 during UNF2, P&O gets reinitialized and relocated to the new LPP having a conductance value less than G_{nom} (0.12) and voltage value above $V_{\text{mpp min}}$ (51.5 V) and thus, identifies the uniform irradiance condition and GMPP. Another key observation evident from the results is that, compared with the PSO method, the proposed algorithm settles to its respective GMPP with much shorter tracking time in both cases. This is due to the initialization of P&O in the linear region of the *I–V* curve that subsequently allows faster convergence. On the other

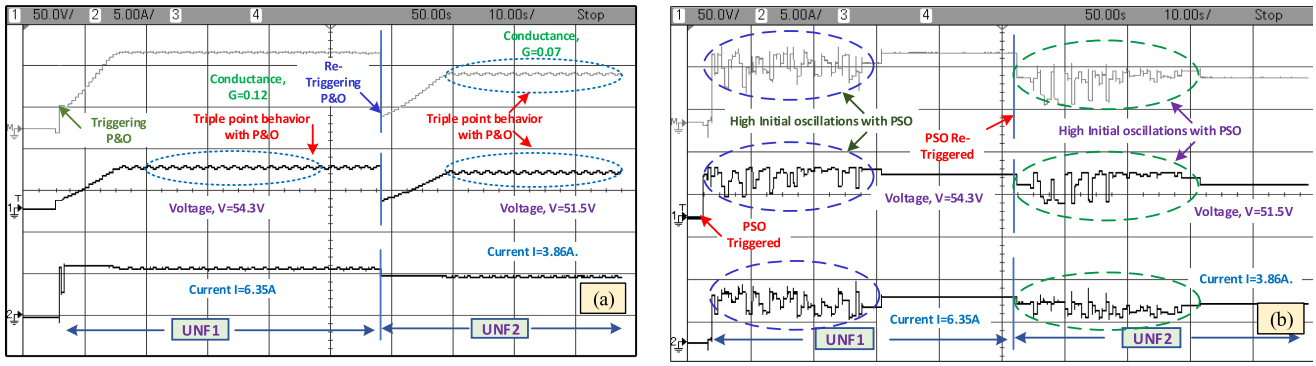

Fig. 8. Experimental results for Test case 1 (3 × 2 PV array)—operational transition from UNF1 to UNF2: (a) proposed, and (b) PSO.

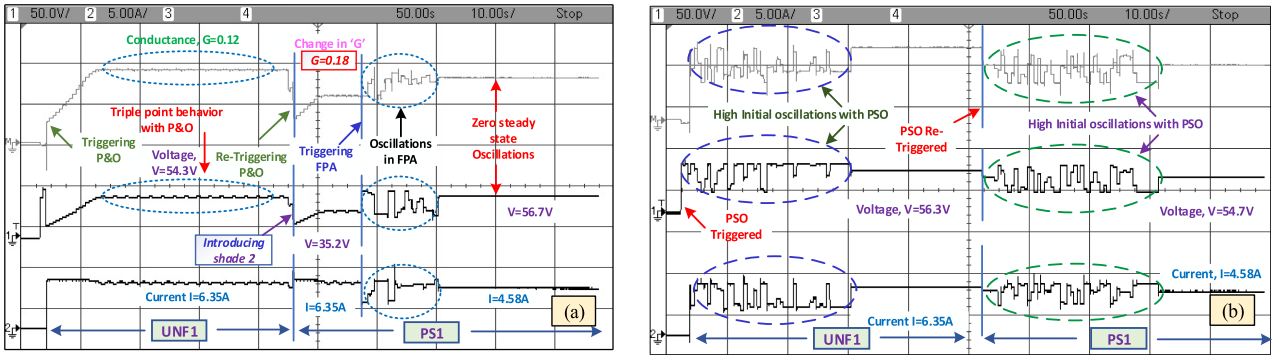

Fig. 9. Experimental results for Test case 2 (3 × 2 PV array)—operational transition from UNF1 to PS1: (a) proposed technique, and (b) PSO.

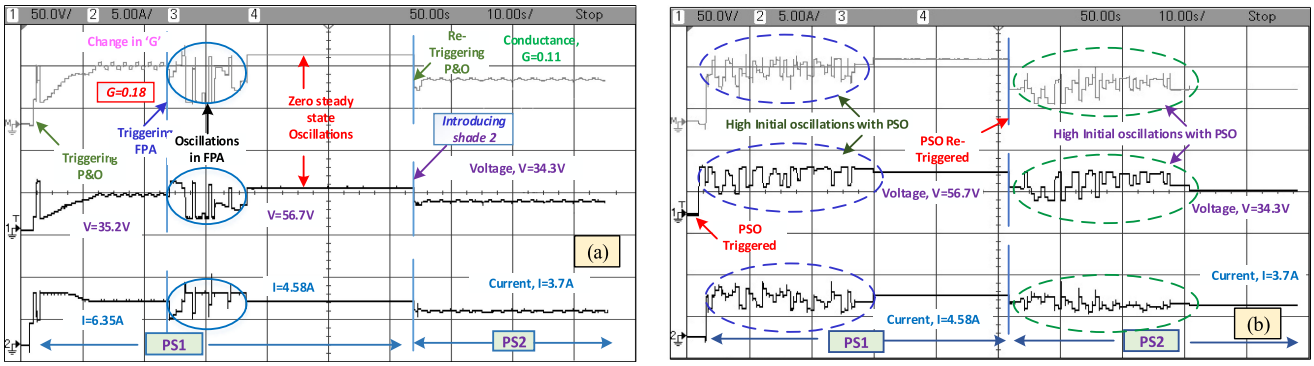

Fig. 10. Experimental results for Test case 3 (3 × 2 PV array)—operational transition from PS1 to PS2: (a) proposed technique, and (b) PSO.

hand, even though PSO tracks GMPP, tracking is characterized by high initial oscillations and slower convergence.

2) Experimental Investigation—Case 2. Operational Transition From UNF1 to PS1: This particular experiment presents a challenging sequence where the array transforms from STC to PSC. Fig. 9(a) and (b) shows the tracking waveforms obtained for the proposed hybrid MPPT and PSO algorithms, respectively. At STC (UNF1), P&O tracks GMPP and operates at nominal conductance and voltage values. When PS1 is introduced at around 50 s, P&O gets reinitialized and locates the nearest LPP at (6.346 A, 35.2 V). As P&O settles to its new operating point, LPP voltage (35.2 V) falls below $V_{\text{mpp min}}$, conductance (0.18) goes beyond G_{nom} and $|\Delta v|$ (19 V) is greater than 0.7 $V_{\text{mpp module}}$. Consequently, the proposed MPPT algorithm detects shade occurrence and as per Table II, the FPA method is initiated to track the GMPP located at (4.577 A, 56.7 V). Justifying its selection, compared with PSO, FPA settles to GMPP within three iterations with less initial oscillations. Moreover, a closer examination of the results reveals that PSO fails to locate GMPP accurately due to the initialization constraints. It is worth mentioning that the results are precisely in line with the findings presented in Tables I and II.

3) Experimental Investigation—Case 3. Operational Transition From PS1 to PS2: The operational transition of the PV array between two PSCs is tested in this sequence. As explained for the previous experiment, for PS1, P&O identifies the occurrence of shade and tracks the GMPP utilizing the FPA method [see Fig. 10(a)]. When PS2 is introduced in sequence to PS1,

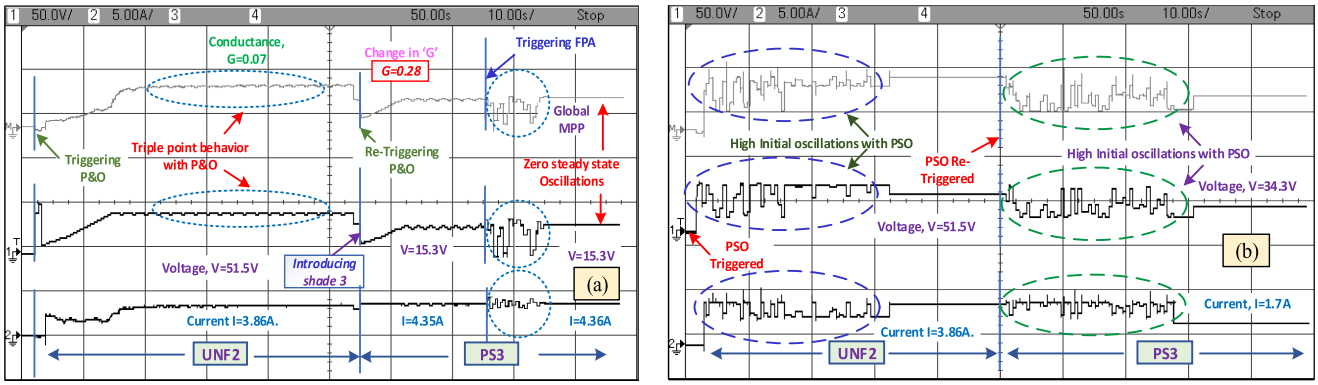

Fig. 11. Experimental results for Test case 4 (3×2 PV array)—operational transition from UNF2 to PS3: (a) proposed technique, and (b) PSO.

P&O tracks the immediate peak with LPP parameters 3.7 A and 34.3 V. It is interesting to note that, alike PS1, PS2 represents a distinct two-peak PSC with LPP as GMPP itself. Pertinent to the earlier findings derived in Tables I and II, for PS2, both P&O conductance and voltage values fall below G_{nom} and $V_{\text{mpp min}}$, and are 0.11 and 34.3 V, respectively. From this peculiar nature of the operating conductance and voltage values at LPP, P&O accurately identifies the occurrence of a two-peak PSC with LPP as GMPP. Subsequently, the need for a further search using FPA is eliminated even if the array is partially shaded and P&O continues to operate at GMPP itself. Unfortunately, though PSO settles to GMPP comfortably in both cases [see Fig. 10(b)], tracking involves delayed convergence and high initial oscillations due to the nonarbitrariness in control variables. Undoubtedly, this experiment demonstrates the efficiency of the proposed algorithm in reducing the power loss involved with the tracking process and is a significant improvement compared to all existing hybrid techniques available in the literature.

4) Experimental Investigation—Case 4. Operational Transition From UNF2 to PS3: The performance of the proposed algorithm during PSCs occurring in low irradiation levels is evaluated via this case study. For which, the array is subjected to PSC while operating at a uniform irradiance of 600 W/m^2. Experimental results obtained in response to the transition from UNF2 to PS3 is plotted in Fig. 11(a) (proposed technique) and Fig. 11(b) (PSO). Identical results as obtained for previously studied case 2 (UNF1–PS1) is perceived here as well. As in case1, P&O easily tracks the unique MPP in uniform irradiance (3.86 A at 51.5 V). While, the introduction of PS3 violates the limits of V, G, and $|\Delta v|$ expressed in Table II (15.3 V, 0.28, and 35 V) even though the respective LPP is GMPP. Therefore, the FPA method is initiated to locate the same LPP once again. Note that identifying GMPP in such extreme shade cases is a tedious task and is beyond the scope of this article. On the other hand, PSO gets trapped to the local maximum at (1.7 A, 34.3 V) and moreover, is characterized by extensive transient power and voltage oscillations as shown in Fig. 11(b).

5) Experimental Investigation—Case 5. Operational Transition From PS1–PS2–PS3: The compatibility of the proposed MPPT scheme during dynamic irradiance variations and its performance in response to such operating conditions is critically analyzed in this case. To authenticate the veracity of the method under dynamic shade conditions, three patterns under partial shade conditions are considered in this sequence. Initially, P&O locates the LPP at (6.3 A, 35.2 V) and monitors the threshold limits to detect the shade occurrence. Once the shade is detected, FPA is triggered to identify the GMPP at (4.57 A, 56.7 V) accurately. At the onset of PS2, P&O is reinitialized to settle to the nearest LPP. Note that, the voltage and conductance limits at this point fall below its threshold limits and thereby P&O identifies the LPP as GMPP, and further search using FPA is avoided [see Fig. 12(a)]. In contrast, in addition to its high oscillations, PSO consumes a longer time to search for GMPP in the entire *I–V* curve [see Fig. 12(b)]. Similar results can also be seen for the second transition of the array from PS2 to PS3 as well, where the proposed algorithm efficiently employs FPA to reach the GMPP (4.36 A, 15.3 V) with minimal oscillations upon detecting the shade. It is evident that the proposed hybrid tracking algorithm eliminates unnecessary switching and thereby, substantially reduces the transient oscillations during dynamic irradiation changes.

B. GMPP Tracking Experiments on a 4×2 PV Array

To generalize the applicability of the proposed technique independent of the PV array size and shade patterns, the experimental investigation is extended to a 4×2 PV array as well. For analysis, the considered 4×2 PV array is built with the same SM 55 PV modules as discussed for earlier experiments. Furthermore, the dynamic tracking capability of the propounded hybrid MPPT algorithm is tested for a combination of sequences having dissimilar string wise irradiance changes. The corresponding *I–V* and *P–V* curves simulated for an effective study are represented in Fig. 13(a) and (b), respectively. These patterns are exclusively studied to analyze the compatibility of the proposed technique to central inverter topologies. As exemplified, three patterns (one uniform and two PSCs) are considered: uniform irradiance STC (UNF), PS1, and PS2. The irradiation profile applied to the PV array to obtain the output characteristics in each case is illustrated in Table V.

1) Dynamic Tracking Test on a 4×2 PV Array: Operational Transition From UNF–PS1–PS2: This particular sequence is specifically chosen to verify that the proposed algorithm performs well under rapid changes in irradiation conditions, responds accurately to all insolation changes irrespective of the type of shading on individual strings, and is compatible for

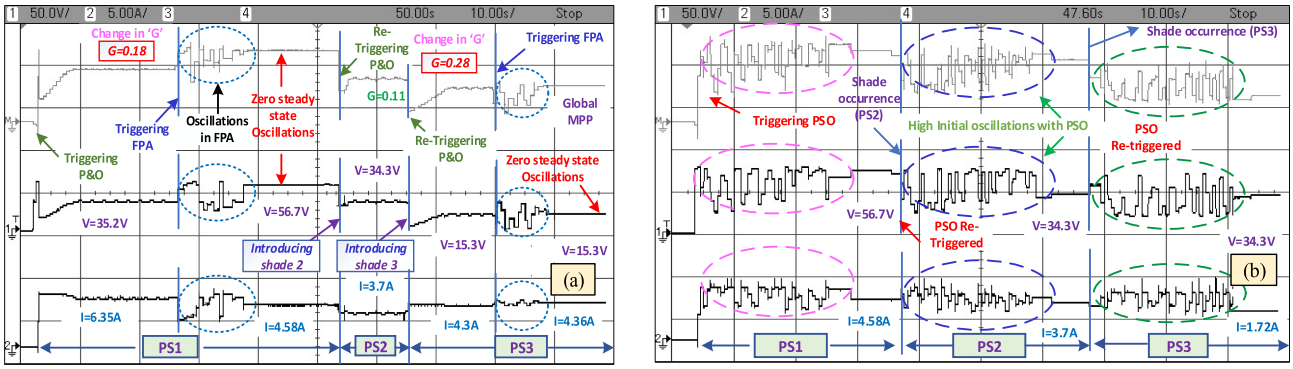

Fig. 12. Experimental results for Test case 5 (3 × 2 PV array)—operational transition from PS1 to PS2 to PS3:proposed and (b) PSO.

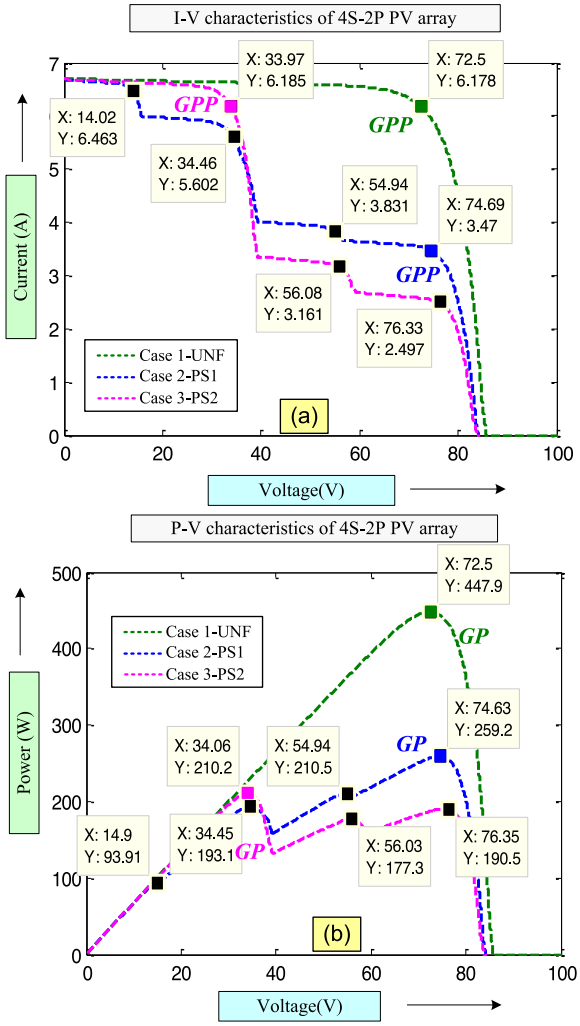

Fig. 13. Different operating conditions considered for a 4 × 2 PV array: (a) *I–V* and (b) *P–V* characteristics.

multiple string PV systems. The resultant waveforms obtained for the proposed technique for the dynamic tracking test is shown in Fig. 14(a). For the considered PV configuration, the threshold values for $V_{\text{mpp min}}$ and G_{nom} is 65 V and 0.087. Now, consider the operation of the developed MPPT strategy. At STC conditions, P&O rapidly identifies uniform irradiance as the voltage and conductance at unique LPP (MPP) (6.35 A, 72.8 V)

TABLE V
IRRADIATION PROFILE FOR A 4 × 2 PV ARRAY

Pattern	Column	Irradiation value in W/m^2			
		Row 1	Row 2	Row 3	Row 4
UNF	C1	1000	1000	1000	1000
	C2	1000	1000	1000	1000
PS1	C1	1000	800	700	600
	C2	1000	1000	500	500
PS2	C1	1000	1000	500	300
	C2	1000	1000	800	300

is $> V_{\text{mpp min}}$ and $\leq G_{\text{nom}}$, respectively. When the insolation profile changes to that of PS1, P&O identifies and tracks the LPP located at (6.4 A, 14.56 V). As both LPP thresholds and $|\Delta v|$ are violated at this point, the algorithm deploys FPA to track the exact GMMP, which settles to 3.44 A at 75.6 V within three iterations with very few oscillations. Similarly, when PS2 is introduced, P&O reinitializes and settles to the LPP at 6.17 A, 33.4 V having identical thresholds as for PS1 to detect the shade occurrence. Upon shade detection, FPA is utilized to accurately track GMPP with minimal transient oscillations. However, in the case of PSO, for each irradiation change, the controller reinitiates a search over the entire *I–V* curve to locate GMPP, which in turn results in substantial power oscillations [refer Fig. 14(b)]. Moreover, PSO fails to track the exact GMPP since the power difference between GMPP and local MPP is very minimal. Undoubtedly, the results confirm the pre-eminence of the proposed algorithm to track GMPP independent of dynamic irradiance changes, PV configuration type, and instantaneous shade profile.

C. Differentiating Uniform Irradiance and PSCs at High Operating Temperatures

As discussed in Section III, to be universally effective, the proposed algorithm must be reliable enough to differentiate nominal irradiance changes from PSCs even at high temperature levels. Therefore, a GMPP tracking test is performed to analyze the performance of the proposed hybrid technique in such conditions. The test is conducted for the same 4 × 2 PV array with *I–V* and *P–V* patterns illustrated in Fig. 4(a) and (b), respectively. Assuming that P&O has not been retriggered up 75 °C at 1000 W/m^2, the following operational transition of the PV array is considered, UNF1–UNF2–PS. The resultant waveforms are shown in Fig. 15. As can be visualized, the initial operating point

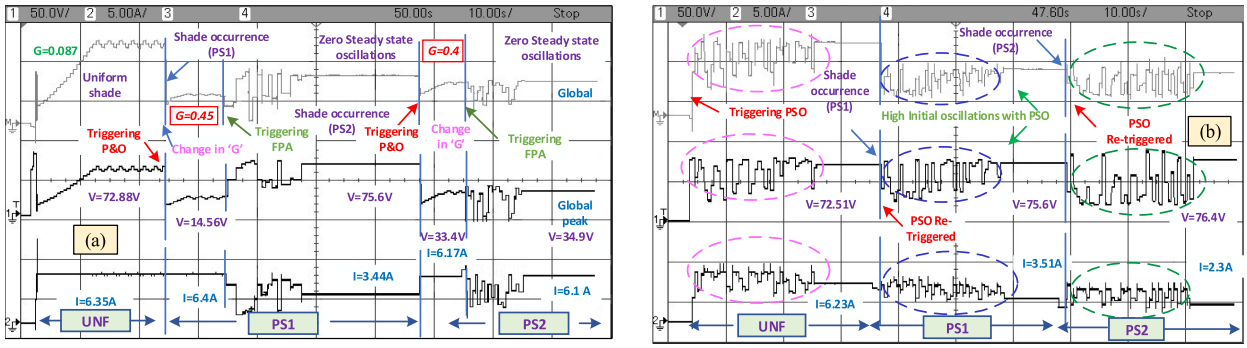

Fig. 14. Dynamic tracking test on a 4×2 PV array—operational transition from UNF to PS1 to PS2: (a) proposed technique, and (b) PSO.

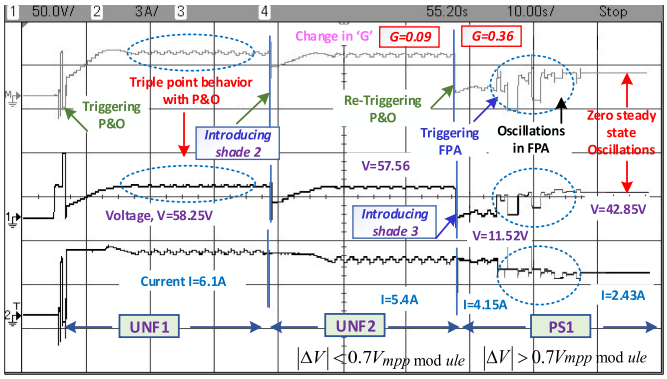

Fig. 15. Demonstrating the effectiveness of the proposed method in high operating temperatures.

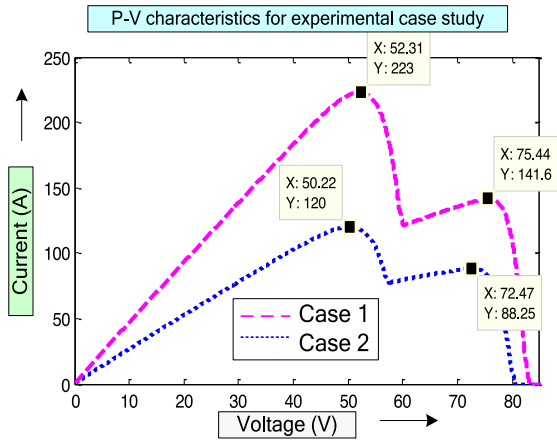

Fig. 16. Two-peak PSCs considered for experimental comparison.

of P&O is (6.1 A, 58.25 V) at 1000 W/m^2. Subsequently, when UNF2 is introduced at the same temperature, both LPP conductance and voltage limits derived as per Table II are violated and are 0.09 and 57.56 V, respectively. Though these thresholds limits are triggered, it can be seen that the controller accurately identifies the transition to uniform irradiance since $|\Delta v|$ ($\sim$1 V) is way less than its threshold limit of $0.7\,V_{\mathrm{mpp\ module}}$. On the other hand, the onset of PS in sequence to UNF2 is characterized by a huge change in $|\Delta v|$ (46 V) that enables the algorithm to initiate FPA to track the GMPP located at (2.43 A, 42.85 V). The results demonstrate the credibility of the developed convention to detect and differentiate PSCs independent of all operating conditions of the PV array.

V. Experimental Comparative Study

To examine the contributions of the proposed methodology to the field of hybrid MPP tracking in PV systems, an experimental study considering some possible practical PSCs is performed. Furthermore, the performance of the proposed strategy is compared with two latest works that are found to be effective and feasible to implement [24]. Experiments are conducted on the 4×2 PV discussed above. After a real-time inspection, two PSCs that often exist in PV arrays are considered for the study and the respective simulated *P–V* curves are shown in Fig. 16. Note that, to emulate a practical scenario, only one row is assumed to be shaded in both cases. Cases 1 and 2 represent PSCs occurring in STC and low insolation levels, respectively.

Now to test the proposed algorithm, the operational transition of the PV array from case 1 to case 2 is considered. PSO–P&O and FWA–P&O [24] are also coded and implemented to portray an effective comparative study. The results obtained for the proposed PSO–P&O and FWA–P&O algorithms are shown in Fig. 17(a)–(c), respectively. It is interesting to note that, for both cases 1 and 2, the proposed method accurately identifies the LPP as GMPP based on the magnitude of LPP voltage ($< V_{\mathrm{mpp\ min}}$) and conductance ($\leq G_{\mathrm{nom}}$) thresholds. Consequently, the use of FPA is eliminated for both cases and is attributed by fast convergence. While, PSO–P&O and FWA–P&O methods consume a larger time to identify GMPP. Moreover, very high switching transients are seen with PSO–P&O tracking strategy and the method is highly complicated due to the addition of the windowing technique. On the other hand, the results portray that the FWA–P&O method has minimal oscillations compared to PSO–P&O. Even then, similar to PSO–P&O, the global search method is essential to track GMPP zones before P&O resumes its operation. The following critical inferences can be concluded based on the study.

1) Compared to existing techniques, the proposed method is highly intelligent to detect PSCs and identify GMPP in practical shade scenarios having two power peaks.
2) The proposed strategy utilizes only conventional P&O to track GMPP in majority of the two-peak PSCs.

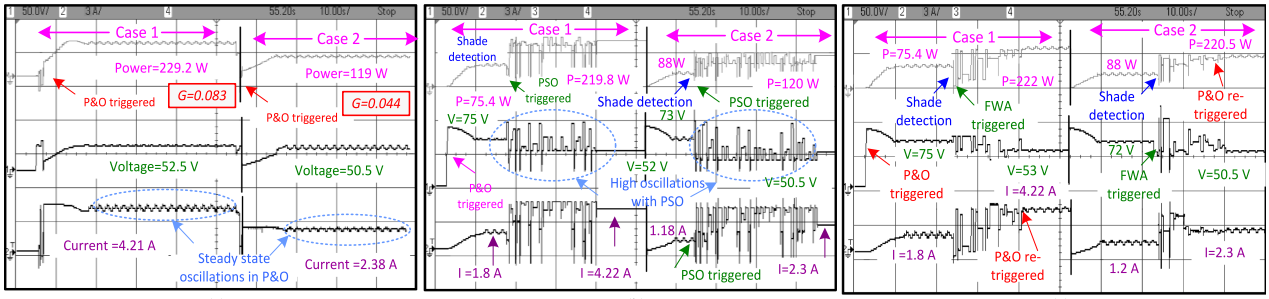

Fig. 17. Experimental comparison—operational transition from case 1 to case 2. (a) Proposed method. (b) PSO-P&O technique. (c) FWA–P&O algorithm.

3) Existing hybrid techniques in the literature are not always accurate to detect shade and the tracking scheme is associated with high switching transients.
4) The proposed technique is principally strong, scalable and easy to implement.

VI. Conclusion

Based on the uniqueness of LPP in an *I–V* curve, a new methodology to detect shade occurrence in PV systems is proposed in this article. Also, evolved from the shade detection approach, a new hybrid MPPT technology was conceptualized, analyzed, tested, and validated. The proposed methodology utilized a combination of conventional P&O and recently evolved FPA for tracking purpose. Extensive experimental evaluations performed in this work revealed that the proposed technique can efficiently track GMPP in all operating conditions of a PV array. Furthermore, as the technique can discriminate the operating conditions of the PV array, the use of the global search algorithm was limited to PSCs only. Even in shade conditions, the selection of FPA to track the GMPP has drastically reduced the transient oscillations owing to its excellent tradeoff between exploration and exploitation processes to search for GMPP. More importantly, the key aspect of the proposed technique is its capability to identify and detect GMPP in PSCs having two power peaks. Therefore, in those cases, the P&O method alone was found suitable to track GMPP. Compared with the techniques in the literature, the proposed technique is accurate, easy to implement and scalable to any PV array size. With the existing techniques in the literature only suitable for string inverters, the proposed algorithm is well suited and can be implemented for both central and string inverters. Overall, the proposed technique is expected to be a viable solution to counteract the disadvantages associated with all existing MPP tracking techniques.

Acknowledgment

The authors would like to thank the Managements NTU-Singapore, NHCE-Bengaluru, Deakin University-Australia and VIT-Vellore for providing their support to carry-out this research work. This work is carried out jointly with the collaboration of Solar Energy Research Cell (SERC), School of Electrical Engineering, VIT-Vellore and the School of Electrical and Electronic Engineering, NTU-Singapore.

References

[1] D. S. Pillai and N. Rajasekar, "A compatibility analysis on NEC, IEC, and UL standards for protection against line–line and line–ground faults in PV arrays," *IEEE J. Photovolt.*, vol. 9, no. 3, pp. 864–871, Mar. 2019.
[2] T. Esram and P. L. Chapman, "Comparison of photovoltaic array maximum power point tracking techniques," *IEEE Trans. Energy Conv.*, vol. 22, no. 2, pp. 439–449, Jun. 2007.
[3] J. P. Ram, T. S. Babu, and N. Rajasekar, "A comprehensive review on solar PV maximum power point tracking techniques," *Renewable Sustain. Energy Rev.*, vol. 67, pp. 826–47, Jan. 2017.
[4] M. Aureliano, L. Galotto, Jr., L. P. Sampaio, G. De Azevedo e Melo, and C. Alberto Canesin, "Evaluation of the main MPPT techniques for photovoltaic applications," *IEEE Trans. Ind. Electron.*, vol. 60, no. 3, pp. 1156–1167, Mar. 2013.
[5] B. Subudhi and R. Pradhan, "A comparative study on maximum power point tracking techniques for photovoltaic power systems," *IEEE Trans. Sustain. Energy*, vol. 4, no. 1, pp. 89–98, Jan. 2013.
[6] H. Patel and V. Agarwal, "Maximum power point tracking scheme for PV systems operating under partially shaded conditions," *IEEE Trans. Ind. Electron.*, vol. 55, no. 4, pp. 1689–1698, Apr. 2008.
[7] M. A. Elgendy, B. Zahawi, and D. J. Atkinson, "Assessment of perturb and observe MPPT algorithm implementation techniques for PV pumping applications," *IEEE Trans. Sustain. Energy*, vol. 3, no. 1, pp. 21–33, Dec. 2011.
[8] A. K. Abdelsalam, A. M. Massoud, S. Ahmed, and P. N. Enjeti, "High-performance adaptive perturb and observe MPPT technique for photovoltaic-based microgrids," *IEEE Trans. Power Electron.*, vol. 26, no. 4, pp. 1010–1021, Apr. 2011.
[9] M. A. Elgendy, B. Zahawi, and D. J. Atkinson, "Operating characteristics of the P&O algorithm at high perturbation frequencies for standalone PV systems," *IEEE Trans. Energy Convers.*, vol. 30, no. 1, pp. 189–198, Mar. 2015.
[10] A. Safari and S. Mekhilef, "Simulation and hardware implementation of incremental conductance MPPT with direct control method using Cuk converter," *IEEE Trans. Ind. Electron.*, vol. 58, no. 4, pp. 1154–1161, Apr. 2011.
[11] G.-C. Hsieh, H.-I. Hsieh, C.-Y. Tsai, and C.-H. Wang, "Photovoltaic power-increment-aided incremental-conductance MPPT with two-phased tracking," *IEEE Trans. Power Electron.*, vol. 28, no. 6, pp. 2895–2911, Dec. 2012.
[12] Y. H. Liu, S. C. Huang, J. W. Huang, and W. C. Liang, "A particle swarm optimization-based maximum power point tracking algorithm for PV systems operating under partially shaded conditions," *IEEE Trans. Energy Convers.*, vol. 27, no. 4, pp. 1027–1035, Dec. 2012.
[13] K. Ishaque, Z. Salam, M. Amjad, and S. Mekhilef, "An improved particle swarm optimization (PSO)-based MPPT for PV with reduced steady state oscillation," *IEEE Trans. Power Electron.*, vol. 27, no. 8, pp. 3627–3638, Aug. 2012.
[14] K. Sundareswaran, S. Peddapati, and S. Palani, "MPPT of PV systems under partial shaded conditions through a colony of flashing fireflies," *IEEE Trans. Energy Convers.*, vol. 29, no. 2, pp. 463–472, Jun. 2014.
[15] K. Sundareswaran, S. Peddapati, and S. Palani, "Application of random search method for maximum power point tracking in partially shadedphotovoltaic systems," *IET Renewable Power Gener.*, vol. 8, no. 6, pp. 670–678, Aug. 2014.

[16] K. Sundareswaran, P. Sankar, P. S. R. Nayak, S. P. Simon, and S. Palani, "Enhanced energy output from a PV system under partial shaded conditions through artificial bee colony," *IEEE Trans. Sustain. Energy*, vol. 6, no. 1, pp. 198–209, Jan. 2015.
[17] J. P. Ram and N. Rajasekar, "A novel flower pollination based global maximum power point method for solar maximum power point tracking," *IEEE Trans. Power Electron.*, vol. 32, no. 11, pp. 8486–8499, Nov. 2017.
[18] D. S. Pillai and N. Rajasekar, "An MPPT based sensorless line-line and line-ground fault detection technique for PV systems," *IEEE Trans. Power Electron.*, vol. 34, no. 9, pp. 8646–8659, Sep. 2019.
[19] K. Ishaque and Z. Salam, "A deterministic particle swarm optimization maximum power point tracker for photovoltaic system under partial shading condition," *IEEE Trans. Ind. Electron.*, vol. 60, no. 8, pp. 3195–3206, Aug. 2013.
[20] K. Sundareswaran, V. Vigneshkumar, P. Sankar, S. P. Simon, P. S. R. Nayak, and S. Palani, "Development of an improved P&O algorithm assisted through a colony of foraging ants for MPPT in PV system," *IEEE Trans. Ind. Inform.*, vol. 12, no. 1, pp. 187–200, 2016.
[21] M. Kermadi, Z. Salam, J. Ahmed, and E. M. Berkouk, "An effective hybrid maximum power point tracker of photovoltaic arrays for complex partial shading conditions," *IEEE Trans. Ind. Electron.*, vol. 66, no. 9, pp. 6990–7000, Sep. 2019.
[22] M. Seyedmahmoudian *et al.*, "Simulation and hardware implementation of new maximum power point tracking technique for partially shaded PV system using hybrid DEPSO method," *IEEE Trans. Sustain. Energy*, vol. 6, no. 3, pp. 850–862, Jul. 2015.
[23] N. Kumar, H. Ikhlaq, B. Singh, and B. K. Panigrahi. "Rapid MPPT for uniformly and partial shaded PV system by using JayaDE algorithm in highly fluctuating atmospheric conditions," *IEEE Trans. Ind. Inform.*, vol. 13, no. 5, pp. 2406–2416, May 2017.
[24] C. Manickam, G. P. Raman, G. R. Raman, S. I. Ganesan and N. Chilakapati, "Fireworks enriched P&O algorithm for GMPPT and detection of partial shading in PV systems," *IEEE Trans. Power Electron.*, vol. 32, no. 6, pp. 4432–4443, Jun. 2017.
[25] J. Ahmed and Z. Salam, "An accurate method for MPPT to detect the partial shading occurrence in a PV system," *IEEE Trans. Ind. Inform.*, vol. 13, no. 5, pp. 2151–2161, Oct. 2017.
[26] A. M. Furtado, F. Bradaschia, M. C. Cavalcanti, and L. R. Limongi, "A reduced voltage range global maximum power point tracking algorithm for photovoltaic systems under partial shading conditions," *IEEE Trans. Ind. Electron.*, vol. 65, no. 4, pp. 3252–3262, Sep. 2017.
[27] M. Boztepe, F. Guinjoan, G. Velasco-Quesada, S. Silvestre, A. Chouder, and E. Karatepe, "Global MPPT scheme for photovoltaic string inverters based on restricted voltage window search algorithm," *IEEE Trans. Ind. Electron.*, vol. 61, no. 7, pp. 3302–3312, Sep. 2013.
[28] K. Chen, S. Tian, Y. Cheng, and L. Bai, "An improved MPPT controller for photovoltaic system under partial shading condition," *IEEE Trans. Sustain. Energy.*, vol. 5, no. 3, pp. 978–985, Apr. 2014.
[29] M. A. Ghasemi, A. Ramyar, and H. Iman-Eini, "MPPT method for PV systems under partially shaded conditions by approximating I–V curve," *IEEE Trans. Ind. Electron.*, vol. 65, no. 5, pp. 3966–3975, Oct. 2017.
[30] D. S. Pillai and N. Rajasekar, "Metaheuristic algorithms for PV parameter identification: A comprehensive review with an application to threshold setting for fault detection in PV systems," *Renewable. Sustain. Energy Rev.*, vol. 82, no. 3, pp. 3503–3525, Feb. 2018.
[31] M. Esteki, B. Poorali, E. Adib, and H. Farzanehfard, "Interleaved buck converter with continuous input current, extremely low output current ripple, low switching losses, and improved step-down conversion ratio," *IEEE Trans. Ind. Electron.*, vol. 62, no. 8, pp. 4769–4776, Jan. 2015.

Dhanup S. Pillai (M'19) received the B.Tech degree in electrical and electronics engineering from Mahatma Gandhi University, Kerala, India, in 2010, the M.E. degree in power electronics and drives from Anna University, Tamil Nadu, India, in 2015, and the Ph.D. degree in electrical engineering from Vellore Institute of Technology, Vellore, India, in 2019.

He is currently a Postdoctoral Research Fellow with the School of Electrical and Electronic Engineering, Nanyang Technological University, Singapore. His research interests include power electronics and its application to renewable energy systems, protection, electrical fault detection and reliability analysis of PV systems, optimization techniques, and energy storage systems.

J. Prasanth Ram received the B.E. degree in electrical and electronics engineering from the Bannari Amman Institute of Technology, Sathyamangalam, India, in 2012, and the M.E. degree in power electronics and drives from the Kumaraguru College of Technology, Coimbatore, India, in 2014, and the Ph.D. degree from Vellore Institute of Technology, Vellore, India, in 2018.

He is currently a Senior Assistant Professor with the New Horizon College of Engineering, Bengaluru, India. His research interests include power electronics, electrical fault detection, optimization techniques, and applications of power electronics in renewable energy systems.

A. M. Y. M. Ghias (S'10–M'14–SM'19) received the B.Sc. degree in electrical engineering from Saint Cloud State University, St. Cloud, MN, USA, in 2001, the M.Eng. degree in telecommunications from the University of Limerick, Limerick, U.K., in 2006, and the Ph.D. degree in electrical engineering from the University of New South Wales (UNSW), Sydney, NSW, Australia, in 2014.

From February 2002 to July 2009, he had held various positions such as Electrical Engineer, Project Engineer, and Project Manager, while working with the top companies in Kuwait. He was with UNSW (2014–2015) and the University of Sharjah, Sharjah, U.A.E (2015–2018). He is currently an Assistant Professor with the School of Electrical and Electronics Engineering, Nanyang Technological University, Singapore. His research interests include model predictive control, hybrid energy storage, renewable energy sources, multiphase drives, novel multilevel converters, and advanced modulations for multilevel converters.

Md Apel Mahmud received the bachelor's degree in electrical engineering, with the University Gold Medal, from Rajshahi University of Engineering and Technology, Rajshahi, Bangladesh, in 2008, and the Ph.D. degree in electrical engineering, with the best thesis award, from the University of New South Wales, Sydney, NSW, Australia, in December 2012.

He is currently a Senior Lecturer of electrical and renewable energy engineering with Deakin University, Geelong, VIC Australia. His research interests include power system stability, control of power systems including renewable energy sources as well as microgrids, energy management for microgrids, energy storage systems, transactive energy (data analytics), and nonlinear control theory.

N. Rajasekar (M'12–SM'19) received the B.E. degree in electrical and electronics engineering from the University of Madras, Chennai, India, in 2000, the M.Tech. degree in power electronics and drives from SASTRA University, Thanjavur, India, 2002, and the Ph.D. degree in electrical engineering from the National Institute of Technology, Trichy, India, in 2007.

From 2005 to 2010, he was working with the Institute of Road and Transport Technology, Erode, India. He is currently a Professor with the Department of Energy and Power Electronics, School of Electrical Engineering, Vellore Institute of Technology, Vellore, India. His research interests include solar PV system, power electronics, application of power electronics in renewable energy sources, and dc–dc converters.

Dr. Rajasekar was the recipient of "Sophia Lecturing—Research Grant," from Sophia University, Tokyo, Japan.